MAP3K4/CBP-Regulated H2B Acetylation Controls Epithelial-Mesenchymal Transition in Trophoblast Stem Cells

Amy N. Abell,[1,2,7,*] Nicole Vincent Jordan,[1,2,7] Weichun Huang,[6] Aleix Prat,[2,4] Alicia A. Midland,[5] Nancy L. Johnson,[1,2]
Deborah A. Granger,[1,2] Piotr A. Mieczkowski,[2,3] Charles M. Perou,[2,4] Shawn M. Gomez,[5] Leping Li,[6]
and Gary L. Johnson[1,2,*]
[1]Department of Pharmacology
[2]Lineberger Comprehensive Cancer Center
[3]Department of Genetics and Carolina Center for Genome Sciences
[4]Department of Genetics
[5]Department of Biomedical Engineering and Curriculum in Bioinformatics and Computational Biology
University of North Carolina School of Medicine, Chapel Hill, NC 27599-7365, USA
[6]Biostatistics Branch, National Institute of Environmental Health Sciences RTP, NC 27709, USA
[7]These authors contributed equally to this work
*Correspondence: amy_abell@med.unc.edu (A.N.A.), gary_johnson@med.unc.edu (G.L.J.)
DOI 10.1016/j.stem.2011.03.008

SUMMARY

Epithelial stem cells self-renew while maintaining multipotency, but the dependence of stem cell properties on maintenance of the epithelial phenotype is unclear. We previously showed that trophoblast stem (TS) cells lacking the protein kinase MAP3K4 maintain properties of both stemness and epithelial-mesenchymal transition (EMT). Here, we show that MAP3K4 controls the activity of the histone acetyltransferase CBP, and that acetylation of histones H2A and H2B by CBP is required to maintain the epithelial phenotype. Combined loss of MAP3K4/CBP activity represses expression of epithelial genes and causes TS cells to undergo EMT while maintaining their self-renewal and multipotency properties. The expression profile of MAP3K4-deficient TS cells defines an H2B acetylation-regulated gene signature that closely overlaps with that of human breast cancer cells. Taken together, our data define an epigenetic switch that maintains the epithelial phenotype in TS cells and reveals previously unrecognized genes potentially contributing to breast cancer.

INTRODUCTION

The transition of epithelial cells to motile mesenchymal cells occurs through a process known as epithelial-mesenchymal transition (EMT), in which epithelial cells lose cell-cell contacts and apical-basal polarity concomitantly with the acquisition of a mesenchymal morphology and invasive properties. Several molecular events are coordinated for the initiation and completion of EMT, including loss of the adhesive cell-surface protein E-cadherin, activation of EMT-inducing transcription factors, and reorganization of the actin cytoskeleton (Yang and Wein-

berg, 2008). During development, EMT is responsible for proper formation of the body plan and for differentiation of many tissues and organs. Examples of EMT in mammalian development include implantation, gastrulation, and neural crest formation (Thiery et al., 2009). Initiation of placenta formation regulated by trophoectoderm differentiation is the first, and yet most poorly defined, developmental EMT.

The commitment of stem cells to specialized cell types requires extensive reprogramming of gene expression, involving, in part, epigenetic control of transcription. The first cell-fate decision is the formation of the trophoectoderm and the inner cell mass of the blastocyst. Trophoblast stem (TS) cells within the trophoectoderm maintain a self-renewing state in the presence of FGF4 (Tanaka et al., 1998). For TS cells and most other tissue stem cells, self-renewal is defined as cell division with the maintenance of multipotency (He et al., 2009). Diminished exposure to FGF4 induces TS cells to give rise to multiple differentiated trophoblast lineages, each required for establishment of the placenta. For implantation to occur, TS cells must undergo morphological changes to a more invasive phenotype, thereby exhibiting the functional hallmarks of EMT.

An emerging topic in the EMT field is the intersection between EMT and stemness. We have previously characterized the developmental defects of a genetically engineered mouse with the targeted inactivation of MAP3K4, a serine-threonine kinase important for JNK and p38 activation in response to FGF4 (Abell et al., 2009). In addition to embryonic defects, the MAP3K4 kinase-inactive mouse (KI4) has trophoblast defects resulting in hyperinvasion, defective decidualization, fetal growth restriction, and implantation defects (Abell et al., 2005, 2009). TS cells isolated from the conceptuses of KI4 mice (TS[KI4] cells) exhibit the hallmarks of EMT, while maintaining TS cell multipotency, and are a unique developmental stem cell model from which to examine parallels between EMT and stemness.

Recently, EMT has been linked to the metastatic progression of cancer and to the acquisition of stem cell properties (Mani et al., 2008). The claudin-low (CL) intrinsic subtype of breast cancer is characterized by its mesenchymal and stem cell-like
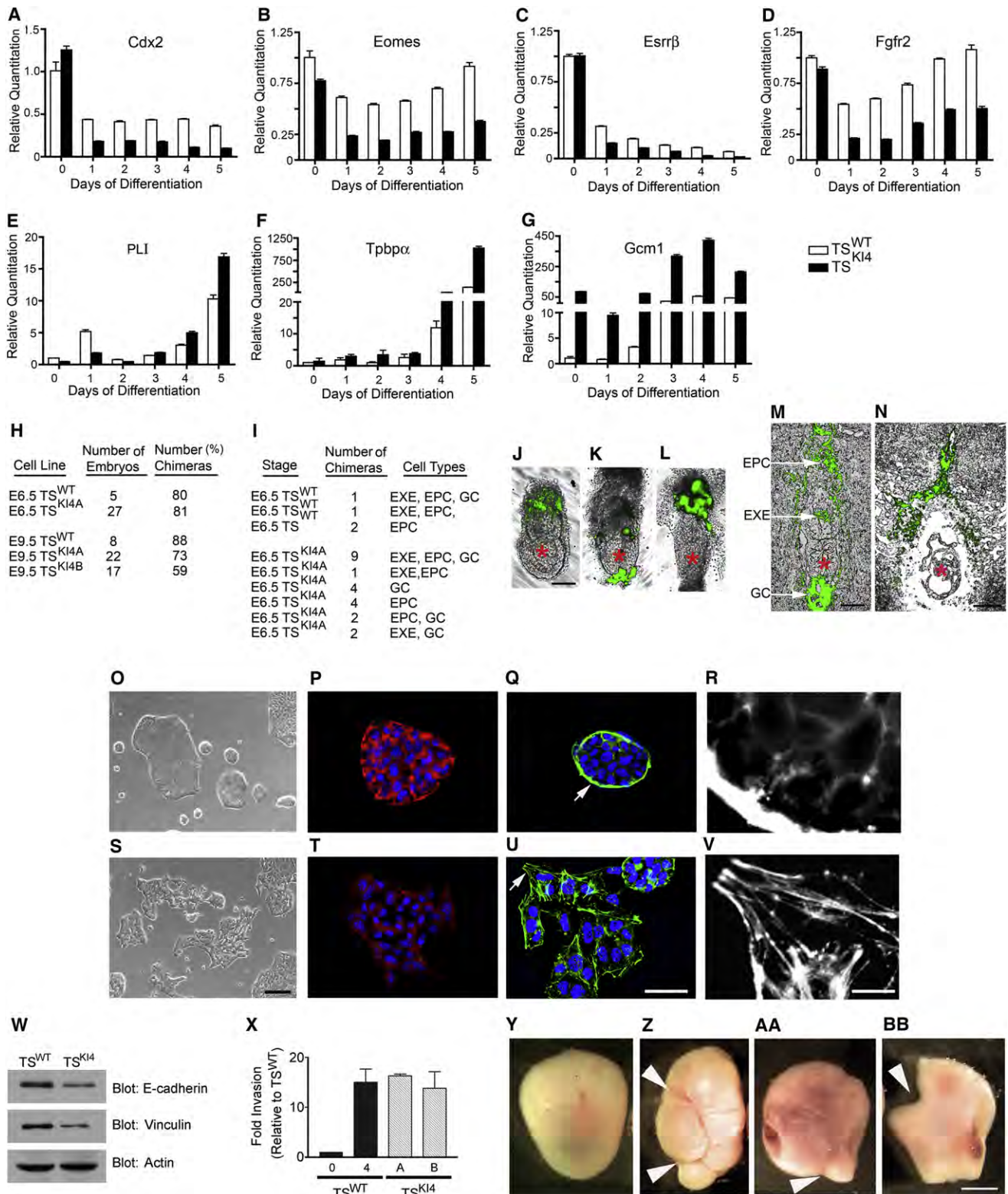
Figure 1. TS^{KI4} Cells Deficient in MAP3K4 Activity Maintain Self-Renewal, Multipotency, and Developmental Potency While Exhibiting Properties of EMT

(A–D) Expression of TS cell stemness genes in TS^{KI4} cells measured by qRT-PCR.

(E–G) Maintenance of multipotency in TS^{KI4} cells demonstrated by induction of trophoblast differentiation markers measured by qRT-PCR. Differentiation was induced by FGF4 withdrawal for the indicated number of days.

properties. In concordance with the stem cell-like CD44$^+$/CD24$^{-/lo}$ and CD49f$^+$/EpCAM$^-$ antigenic phenotypes of breast tumor-initiating cells (TICs) and mammary stem cells, gene-expression profiling demonstrated that CL tumors have reduced expression of several epithelial differentiation markers, while exhibiting increased expression of certain stemness and mesenchymal markers (Lim et al., 2009; Prat et al., 2010).

Herein, we define an epigenetic mechanism important for the initiation of the first EMT event during development. Using TS^{KI4} cells uniquely trapped in EMT prior to initiation of the trophoblast differentiation program, we capture the genetic and epigenetic profile of the intersection between the properties of EMT and stemness. Importantly, we identify a molecular mechanism reliant on the histone acetyltransferase CBP that is responsible for controlling epigenetic remodeling during EMT in TS^{KI4} cells. TS cells lacking CBP (TS^{shCBP}) expression exhibit an EMT similar to TS^{KI4} cells, which is mediated by the selective loss of H2A and H2B acetylation. Comparison across developmental and cancer EMT models exhibiting stem-like properties demonstrated a highly significant intersection between the gene expression profiles of TS^{KI4} cells and CL human tumors and cell lines. Repressed genes from the EMT gene signature demonstrated loss of H2BK5Ac in TS^{KI4}, TS^{shCBP}, and CL cells. These results highlight the importance of MAP3K4/CBP-mediated acetylation of H2BK5 for maintenance of the TS cell epithelial phenotype.

RESULTS

TS^{KI4} Cells Exhibit Properties of Both Stemness and EMT

In the presence of FGF4, TS cells maintain self-renewal as defined by the maintenance of cell division with multipotency (Niwa et al., 2005; Tanaka et al., 1998). TS^{KI4} cells lack MAP3K4 activity but are self-renewing and multipotent. When cultured in the presence of FGF4, TS^{KI4} cells expressed the TS cell markers Cdx2, Eomes, Esrrβ, and FGFR2 at levels similar to TS^{WT} cells (Figures 1A–1D). Removal of FGF4 promoted the differentiation of TS^{KI4} cells into all trophoblast lineages similar to TS^{WT} cells with the loss of expression of stem cell markers (Figures 1A–1D) and the gain of expression of trophoblast lineage markers, including the giant cell marker PLI, the spongiotrophoblast marker Tpbpα, and the syncytiotrophoblast marker Gcm1 (Figures 1E–1G). Developmental potency of these stem cells was established through the injection of GFP-labeled TS^{WT} or TS^{KI4} cells into wild-type blastocysts. Both TS^{WT} and TS^{KI4} cells produced chimeric conceptuses with similar frequencies (Figure 1H) and contributed selectively to the trophoblast lineages, including the extraembryonic ectoderm, ectoplacental cone, and giant cells (Figures 1I–1N and see Figures S1A–S1H available online). These cells were not found in the embryo or in any ICM-derived extraembryonic tissue (Figures 1I–1N).

TS^{KI4} cells also exhibit the molecular and cellular characteristics of EMT. TS^{WT} cells grew with an epithelial morphology (Figure 1O), strong peripheral E-cadherin (Figure 1P), and cortical actin expression at cell-cell contacts (Figures 1Q and 1R). In contrast, TS^{KI4} cells exhibited a polarized front-back end, mesenchymal morphology (Figure 1S). E-cadherin was significantly reduced in TS^{KI4} cells (Figure 1T). Also, filamentous actin was observed at the leading edge of TS^{KI4} cells (Figures 1U and 1V). Reduction of total E-cadherin in TS^{KI4} cells relative to TS^{WT} cells was further validated by western blotting (Figure 1W). Real-time quantitative RT-PCR (qRT-PCR) showed a modest increase in the expression of the mesenchymal markers vimentin and N-cadherin in TS^{KI4} cells, and western blotting revealed a 2.9- and 2.2-fold increase in vimentin and N-cadherin protein expression respectively (Figures S1I and S1J). Differentiation of both TS^{WT} and TS^{KI4} cells also increased vimentin and N-cadherin protein expression (Figure S1J). TS^{KI4} cells and 4 day differentiated TS^{WT} cells exhibited a 14- to 16-fold increase in invasiveness compared to TS^{WT} cells (Figure 1X). Hyperinvasiveness of the TS^{KI4} cells was also seen in vivo. Defective decidualization is induced by excessive trophoblast invasion (Norwitz et al., 2001). Compared to injection of TS^{WT} cells (Figure 1Y), injection of TS^{KI4} cells into wild-type blastocysts resulted in defective decidualization consistent with the hyperinvasiveness of TS^{KI4} cells (Figures 1Z–1BB). Cumulatively, these data demonstrate that TS^{KI4} cells are self-renewing stem cells with properties of EMT, including loss of E-cadherin and gain of invasiveness.

Developmental EMT in TS^{WT} Cells

Removal of FGF4 promotes the differentiation of TS cells and increased invasiveness of trophoblasts through Matrigel-coated transwells (Figure 2A). The invasive population was largest at 4 days post FGF4 withdrawal (T^{INV}) (Figure 2A). Morphologically,

(H–N) Developmental potency of TS^{WT} and TS^{KI4} cells demonstrated by injection of GFP positive TS^{WT} and TS^{KI4} cells into wild-type blastocysts. (H) Data show the number of GFP positive chimeras per cell type injected expressed as a percent of total embryos examined. (A) and (B) are two independent TS^{KI4} cell clones. (I) Sites of incorporation of GFP positive TS^{WT} and TS^{KI4} cells in E6.5 conceptuses. (J–L) Three representative whole-embryo E6.5 TS^{KI4} chimeras and (M) 18 μm section from E6.5 TS^{KI4} chimera are shown. Black bar represents 100 μm. EPC, ectoplacental cone; EXE, extraembryonic ectoderm; GC, giant cells. (N) Representative E9.5 TS^{WT} cell chimera. Red asterisks indicate location of embryos.

(O–V) Mesenchymal phenotype of TS^{KI4} cells compared to epithelial morphology of TS^{WT} cells. (O) Phase microscopy of TS^{WT} cells. (P) Immunostaining with anti-E-cadherin antibody (red) shows strong staining around the cellular periphery in TS^{WT} cells with nuclear DAPI stain (blue). (Q) Cortical actin staining (green) and nuclear DAPI stain (blue) in TS^{WT} cells. (R) Enlarged inset of region indicated by arrow in (Q) showing peripheral cortical actin in TS^{WT} cells. (S) Phase microscopy of TS^{KI4} cells. Black bar represents 100 μm. (T) Relocalization and loss of E-cadherin (red) from the periphery of TS^{KI4} cells with nuclear DAPI stain (blue). (U) Filamentous actin staining (green) and nuclear DAPI stain (blue) in TS^{KI4} cells. White bar represents 50 μm. (V) Enlarged inset of region indicated by arrow in (U) showing filamentous actin in TS^{KI4} cells. White arrow indicates site for insets in (R) and (V).

(W) Reduced protein expression of E-cadherin and vinculin in TS^{KI4} cells shown by western blotting.

(X) Invasion through Matrigel by undifferentiated TS^{WT} cells (0), TS^{WT} cells differentiated for 4 days by FGF4 removal (4), or two independent TS^{KI4} cell clones (A and B) cultured in the presence of FGF4. Fold change is relative to TS^{WT} cells.

(Y) Representative E9.5 decidua from blastocyst injected with TS^{WT} cells.

(Z–BB) Three representative E9.5 deciduas from blastocysts injected with TS^{KI4} cells. Arrowheads indicate sites of defective decidualization. (A–G) and (X) represent the mean ± range of two independent experiments.
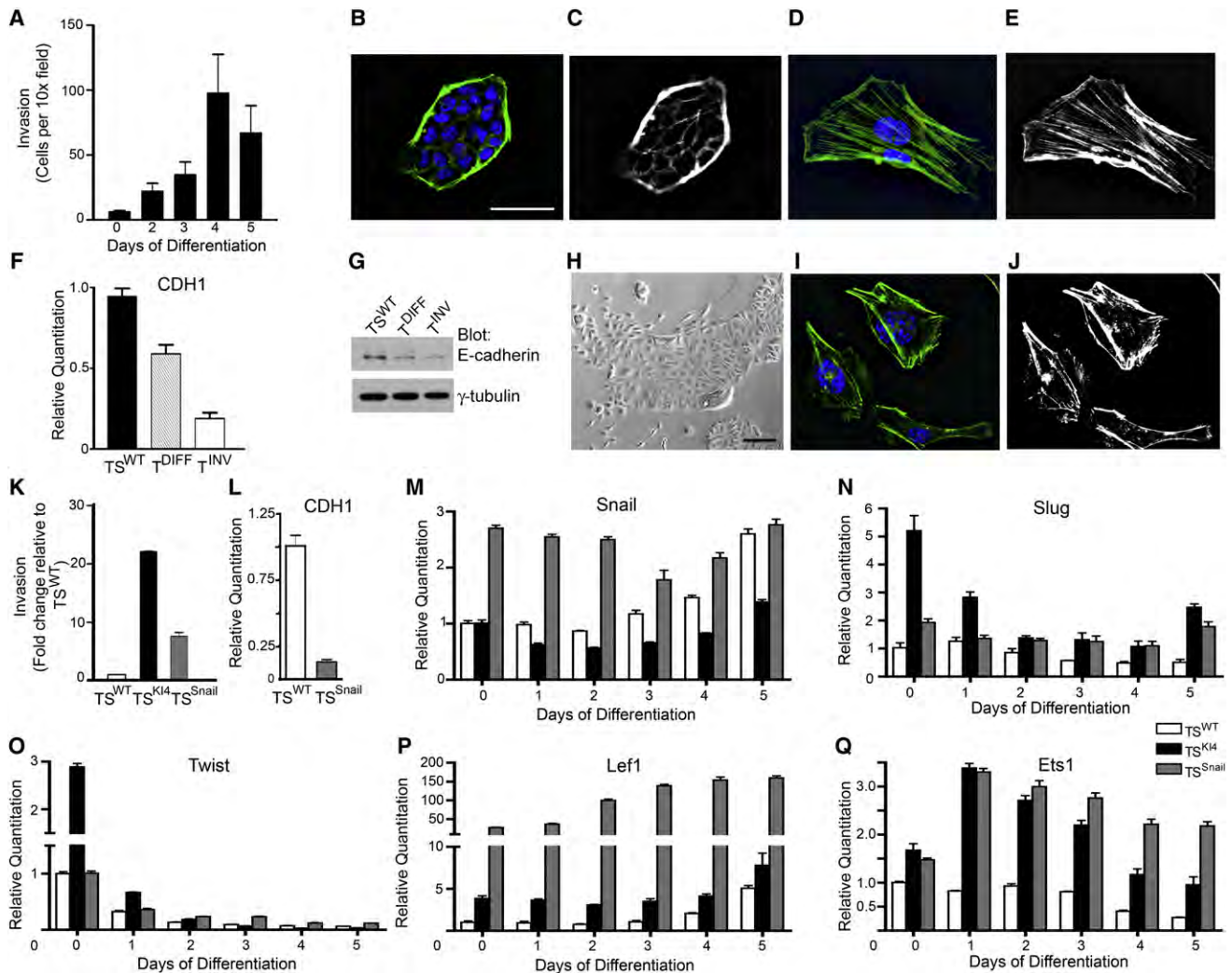
Figure 2. Differentiation of TS^{WT} Cells Induces EMT

(A) Differentiation of TS cells results in increased invasiveness. Invasion through Matrigel by undifferentiated TS cells (0) or TS cells differentiated by FGF4 withdrawal for the indicated number of days (2–5) is shown. Data are the mean ± range of two independent experiments performed in duplicate.

(B–E) Undifferentiated cells (B and C) or invasive cells isolated from the bottom of Matrigel-coated transwell chambers (D and E) plated on glass coverslips. (B and D) Cells were stained for actin (green) and nuclei (blue). (C and E) Actin staining alone shows peripheral cortical actin in undifferentiated cells (C) and filamentous actin in invasive trophoblasts (E). White bar represents 50 μm.

(F) Reduced Cdh1 message (E-cadherin) in invasive trophoblasts (T^{INV}) compared to undifferentiated TS cells (TS^{WT}) and TS cells differentiated for 4 days (T^{DIFF}) measured by qRT-PCR. Data normalized to TS^{WT} samples represent the mean ± SEM of three independent experiments.

(G) Reduced E-cadherin protein in T^{INV} cells shown by western blotting.

(H) Phase microscopy shows mesenchymal morphology of TS^{Snail} cells. Black bar represents 100 μm.

(I) Filamentous actin staining (green) and nuclear DAPI stain (blue) in TS^{Snail} cells.

(J) Filamentous actin staining alone in TS^{Snail} cells is shown.

(K) Increased invasiveness of TS^{KI4} and TS^{Snail} cells relative to TS^{WT} cells is shown.

(L) Reduced Cdh1 message in TS^{Snail} cells compared to TS^{WT} cells is measured by qRT-PCR.

(M–Q) Expression of EMT-inducing genes in TS^{WT}, TS^{KI4}, and TS^{Snail} cells measured by qRT-PCR is shown. Data show the mean ± range of two independent experiments.

TS^{WT} cells cultured in FGF4 grew in tight epithelial sheets with actin localized around the cell periphery (Figures 2B and 2C). In contrast, T^{INV} cells isolated from the bottom of Matrigel-coated transwells exhibited mesenchymal cell characteristics with prominent actin stress fibers and filamentous actin localized to the front end of polarized cells (Figures 2D and 2E) and loss of E-cadherin (Figures 2F and 2G). E-cadherin was more signifi-

cantly reduced in T^{INV} cells compared to 4 day differentiated trophoblasts (T^{DIFF}) not selected for invasiveness (Figures 2F and 2G). Expression of the mesenchymal marker fibronectin was significantly increased and vimentin was also expressed in T^{INV} cells (Figure S2A). These changes in invasiveness, morphology, and E-cadherin expression indicated that the T^{INV} cells have undergone EMT.

Induction of EMT in TS^WT Cells by Ectopic Expression of Snail

To induce EMT in TS cells, we ectopically expressed a defined inducer of EMT, the transcription factor Snail, in TS^{WT} cells (TS^{Snail}) (Cano et al., 2000). TS^{Snail} cells exhibited a polarized, mesenchymal morphology with increased filamentous actin and mesenchymal markers vimentin and N-cadherin (Figures 2H–2J and Figure S2B). A 10-fold increase in invasiveness compared to TS^{WT} cells and loss of E-cadherin showed Snail overexpression-induced TS cell EMT (Figures 2K and 2L). TS^{Snail} cells expressed TS stem cell markers and were able to differentiate into trophoblast lineages upon removal of FGF4 (Figures S2C and S2D). To identify transcription factors responsible for inducing EMT in TS cells, we compared the expression levels of eight transcription factors known to regulate EMT in other systems. FGF4 withdrawal from TS^{WT} cells induced Snail message at 4 days of differentiation and in T^{INV} cells, suggesting that Snail is important for TS cell EMT (Figure 2M and Figure S2E). The EMT-inducing transcription factors Slug and Twist were elevated in undifferentiated TS^{KI4} cells, but were not induced with differentiation or invasion of TS^{WT} cells (Figures 2N and 2O and Figure S2E). Upregulation of Lef1 and Ets1 were also detected in TS^{KI4} and TS^{Snail} cells (Figures 2P and 2Q). Similar to Snail, Lef1 was induced at 4 days of TS^{WT} cell differentiation and in T^{INV} cells (Figure 2P and Figure S2E). Other known transcriptional regulators of EMT, such as Zeb1, Foxc2, and Gsc, were not induced with EMT of T^{INV} or TS^{KI4} cells (Figures S2F–S2H).

Gene Expression Changes with the Acquisition of Trophoblast Invasiveness

To identify genes related to the acquisition of invasiveness in trophoblast EMT, we measured gene expression changes in T^{INV} cells compared to TS^{WT} cells using genome-wide Agilent microarrays. With a Benjamini-Hochberg p value < 0.05, 6641 genes exhibited a minimum 2-fold change in expression in T^{INV} cells (Table S1). Since T^{INV} cells were differentiated for 4 days, a component of the 6641 changed genes reflected differentiation-specific changes unrelated to the acquisition of invasiveness. When gene expression changes of T^{DIFF} cells compared to TS^{WT} cells were measured, 5706 genes exhibited altered expression by a minimum of 2-fold (Table S1). Direct comparison of gene expression changes in T^{INV} and T^{DIFF} cells revealed that 2359 genes had significantly different expressions measured as a minimum 1.5-fold change with 80% of these genes being changed only in T^{INV} cells (Table S2). Gene ontology (GO) analysis of the 2359 genes showed significant enrichment in canonical KEGG pathways regulating focal adhesions, actin cytoskeleton, and adherens junctions (Figure S3A). These findings define an invasive gene signature for trophoblast EMT.

Gene Expression Changes in TS^KI4 Cells

Unlike T^{INV} cells that have undergone EMT, but have lost stemness, TS^{KI4} cells are self-renewing stem cells in EMT. TS^{KI4} cells serve as a useful model to distinguish between genes that mediate invasiveness and EMT. Gene expression profiling defined changes in TS^{KI4} cells compared to TS^{WT} cells, identifying 1083 significantly upregulated genes and 702 significantly downregulated genes by more than 2-fold (Benjamini-Hochberg p value < 0.05) (Table S1). GO analysis of downregulated genes

showed a significant enrichment in nine canonical signaling pathways (Figure S3B). The top three enriched signaling pathways included focal adhesions, ECM-interactions, and regulation of the actin cytoskeleton—the same pathways that were identified in the T^{INV} signature.

Comparison of TS^KI4 and T^INV Signatures Identify Genes Important for EMT

Unsupervised hierarchical clustering of TS^{KI4}, T^{INV}, and T^{DIFF} cells showed a common gene set for T^{INV} and T^{DIFF} cells indicated by a node correlation coefficient of 0.82 (Figure 3A). This strong correlation reflects the significant changes in gene expression due to FGF4 removal and loss of stemness in T^{INV} and T^{DIFF} cells, as compared to TS^{KI4} cells, showing that TS^{KI4} cells are not differentiated cells. Venn diagrams of upregulated (Figure 3B) and downregulated (Figure 3C) genes highlight the significant intersection between T^{DIFF} and T^{INV} cells, while demonstrating the limited intersection of 416 genes between TS^{KI4} and T^{INV} cells. Significantly changed genes were categorized according to biological function, and 25% of these genes regulate cell adhesion and motility, including Lamb2, Fn1, and RhoB (Figure 3D and Figure S3C). In addition, genes were identified whose importance to invasion and EMT has not been previously defined, including the enrichment for genes regulating RNA splicing, transcription, translation, and protein degradation (Figure S3C). However, these genes must be functionally tested to prove their role in invasion and EMT. Using qRT-PCR, we validated the expression changes of several genes showing similar changes in TS^{KI4} and T^{INV} cells (Figures S3D and S3E).

Acetylation of Specific H2A and H2B Lysines Is Inhibited in TS^KI4 Cells

Induction of differentiation by FGF4 removal from TS^{WT} cells was accompanied by reduced acetylation of all core histones, specifically at H2AK5, H2BK5/K12/K15/K20, H3K9, and H4K8 (Figure 4A). Trimethylation of H3K4 and H3K9 was unchanged with differentiation (data not shown). The differentiation-induced loss of histone acetylation suggests the importance of histone acetylation in maintaining the undifferentiated epithelial state of TS cells. We therefore examined histone modifications in TS^{KI4} cells. Figure 4B shows the loss of acetylation at H2AK5, H2BK5, H2BK12, and H2BK15 in TS^{KI4} cells compared to TS^{WT} cells. H3K9Ac and H4K8Ac were unaffected, demonstrating that loss of histone acetylation was selective for H2A and H2B. Examination of histone methylation showed that trimethylation of H3K4 and H3K9 was not altered, suggesting that loss of H2A and H2B acetylation (H2A/H2BAc) in TS^{KI4} cells occurs independently of changes in histone methylation (Figure 4C). Examination of TS^{Snail} cells that exhibit properties of stemness and EMT similar to TS^{KI4} cells revealed the selective loss of H2A/H2BAc with no change in H3 and H4 acetylation (Figure 4D). These data show the association of loss of H2A/H2BAc with changes characteristic of EMT, while maintaining stemness in TS^{KI4} cells.

Reduction of H2BK5Ac on Select Gene Promoters in TS^KI4 Cells

We used ChIP-seq to identify genes associated with the epigenetic mark H2BK5Ac during TS cell reprogramming important for the induction of EMT. After obtaining DNA samples by ChIP
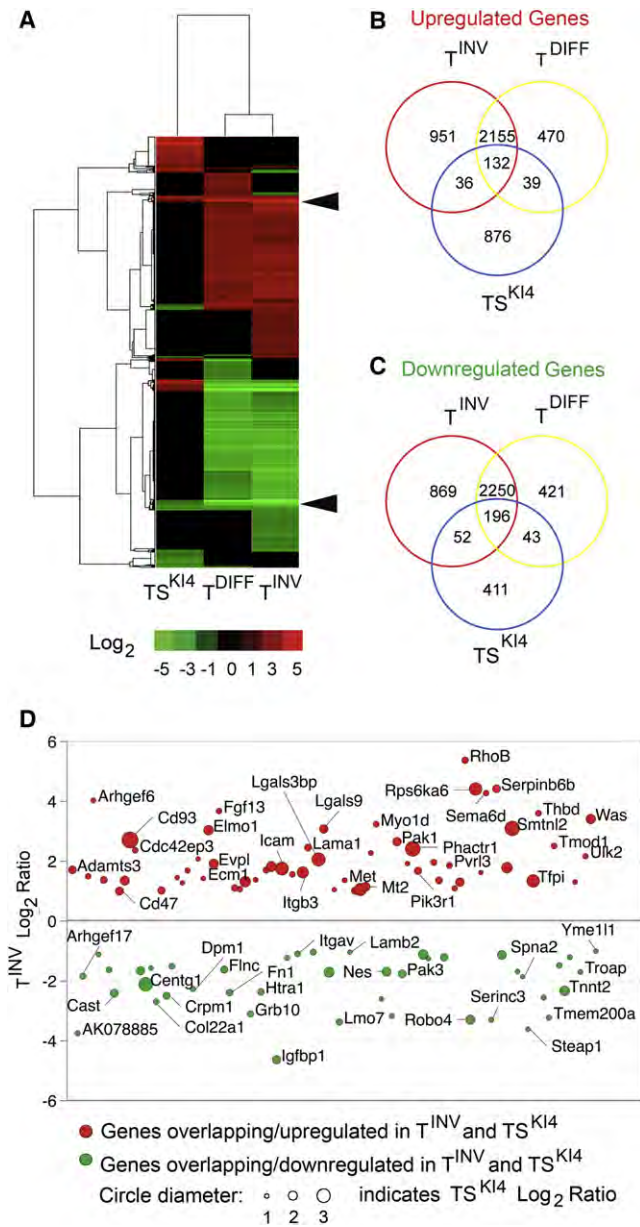
Figure 3. Gene Expression Profiling of EMT in TS^{KI4} Compared to T^{INV} Cells

(A) Loss of MAP3K4 activity in TS^{KI4} cells results in significant changes in gene expression. Heat map compares gene expression changes in TS^{KI4} cells (1785 genes), T^{DIFF} cells (5706 genes), and T^{INV} cells (6641 genes) relative to TS^{WT} cells. Significantly changed genes have a Benjamini-Hochberg p value < 0.05 and log$_2$ ratio ≥ abs (1). Arrowheads indicate overlapping genes.

(B and C) Venn diagrams show the overlap of upregulated (B) and down-regulated (C) genes in TS^{KI4} cells (blue), T^{DIFF} cells (yellow), and T^{INV} cells (red).

(D) Twenty-five percent of the overlapping genes between TS^{KI4} and T^{INV} EMT models control cell adhesion and motility. Diagram depicts T^{INV} cell log$_2$ ratios from (A) for genes that regulate adhesion and motility having shared changes between TS^{KI4} and T^{INV} cells. Circle diameter depicts changes in TS^{KI4} cell log$_2$ ratios.
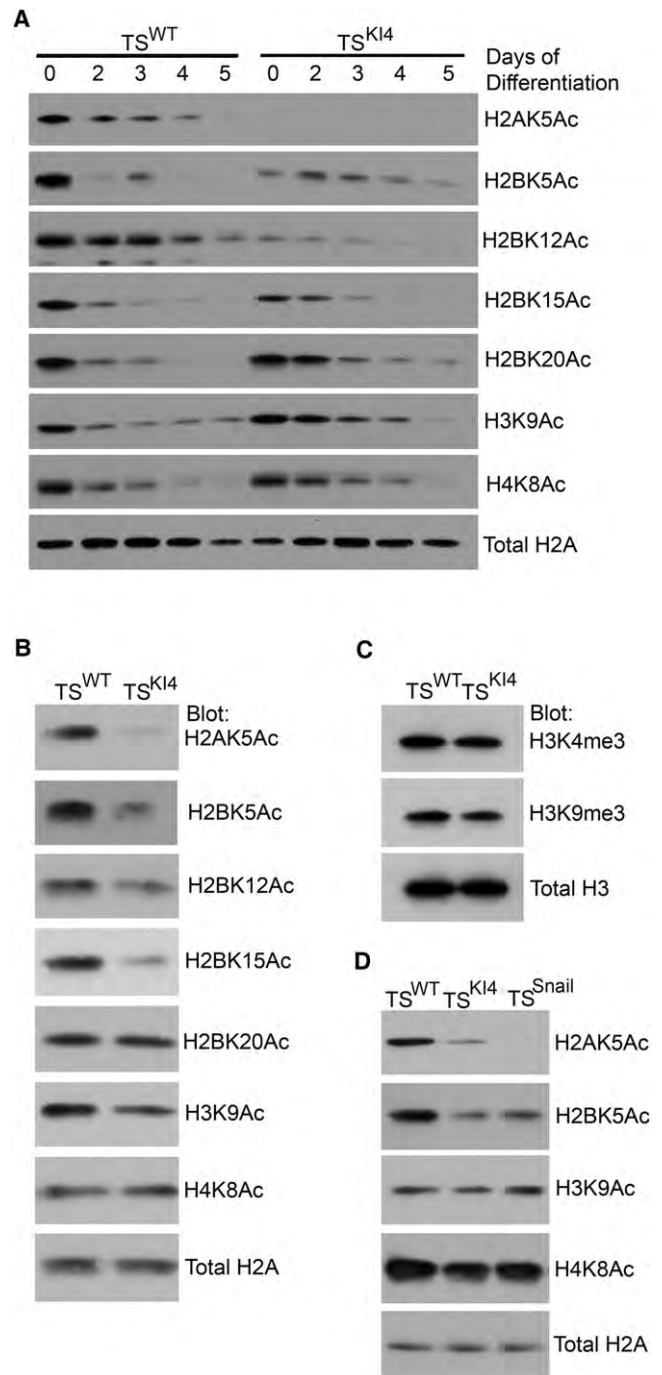

Figure 4. Selective Loss of H2A and H2B Acetylation in Undifferentiated TS^{KI4} Cells

(A) Acetylation of histones H2A, H2B, H3, and H4 is decreased upon induction of TS cell differentiation via withdrawal of FGF4. Western blotting of lysates from TS^{WT} or TS^{KI4} cells differentiated for the indicated days is shown.

(B and C) TS^{KI4} cells exhibit selective loss of acetylation on histones H2A and H2B and no change H3 methylation. Western blots were performed as described for (A).

(D) TS^{Snail} cells exhibit selective loss of acetylation on histones H2A and H2B. Results in (A–D) are representative of two to three independent experiments.

using a highly specific H2BK5Ac antibody (Figures S4A and S4B), we generated a total of 44 and 27 million Illumina sequence reads for TS^{WT} and TS^{KI4} cells respectively, consistent with western blotting data (Figure 4). This genome-wide analysis of the read-tag distribution demonstrated that H2BK5Ac is significantly enriched near the transcription start sites (TSS) of 13,625 genes in TS cells (Table S3 and Figure 5A). This H2BK5Ac peak location profile near the TSS is consistent with published studies in CD4$^+$ T cells (Wang et al., 2008).

Limiting the analysis to the well-annotated RefSeq gene set (NCBI37/mm9), we compared the read tag density between TS^{WT} and TS^{KI4} cells within 1 kb upstream and downstream of the TSS. We normalized read-tag counts based upon the ratio of genome-wide total mapped reads between TS^{WT} and TS^{KI4} cells. We removed background regions by filtering genes whose read tag counts did not significantly exceed cell-type-specific background noise (<20 read tags per 2 kb region). After removing duplicate genes, 4163 genes were significantly different in H2BK5Ac between TS^{WT} and TS^{KI4} cells, as determined by the exact rate ratio test with Benjamini-Hochberg adjusted p value ≤ 0.05. From the 4163 genes with a significant change in H2BK5Ac, 3515 genes had a significant loss of H2BK5Ac, while 648 genes had a significant gain of H2BK5Ac in TS^{KI4} compared to TS^{WT} cells (Figures 5B and 5C).

Changes in H2BK5Ac were visualized by normalized read tag density plots. We demonstrated the dramatic loss of H2BK5Ac in TS^{KI4} cells for a select set of genes including Acsl6, Dbndd2, Itgav, Krt19, and Trim54 (Figure 5D and Figure S4C). These are examples of genes with a highly significant loss of H2BK5Ac (i.e., Benjamini-Hochberg p values < 10^{-18}), and they occur in the top 3% of affected genes (Table S3). Loss of H2BK5Ac in TS^{KI4} compared to TS^{WT} cells was confirmed by ChIP-qRT-PCR (Figure 5E) and correlated with the loss of gene expression (Table S2 and Figure S3E). Furthermore, Acsl6, Itgav, Lamb2, and Trim54 demonstrated a similar loss of H2BK5Ac in T^{INV} cells by ChIP-qRT-PCR, suggesting the importance of these genes in regulating the EMT program that occurs during trophoblast differentiation (Figure 5E). Although the majority of genes had a loss of H2BK5Ac in TS^{KI4} compared to TS^{WT} cells, 648 genes had an increase in H2BK5Ac density in TS^{KI4} cells. Normalized density plots of Dkk3 and Mycn highlight two genes with a significant increase in H2BK5Ac (i.e., Benjamini-Hochberg p values < 10^{-12}) and a coordinate increase in gene expression in TS^{KI4} cells (Figure 5F; Table S1 and Table S3).

Consistent with the maintenance of TS cell multipotency, enrichment of H2BK5Ac occurs at the promoters of the TS cell markers Cdx2, Eomes, and Fgfr2 (Figure 5G). As indicated from normalized promoter density plots, Eomes and Esrrβ demonstrated unchanged levels of H2BK5Ac between TS^{WT} and TS^{KI4} cells, while Cdx2 and Fgfr2 demonstrated a 50% decrease in H2BK5Ac density (Figure 5G). H2BK5Ac levels were validated by H2BK5Ac ChIP-qRT-PCR for the Eomes and Cdx2 promoters (Figure S4D).

Loss of H2BK5Ac Correlates with Repression of Genes Critical to Maintenance of the TS Cell Epithelial Phenotype
Using mRNA-seq to quantitatively compare the changes in H2BK5Ac with the changes in gene expression for TS^{WT} and

TS^{KI4} cells, there was a modest positive correlation between changes in gene expression and H2BK5Ac, as determined by a Pearson correlation coefficient of 0.62 (p value < 10^{-16}) (Figure 5H). This finding was further supported by GO analysis of genes both significantly downregulated and hypoacetylated, showing shared gene changes important for maintenance of focal adhesions, the actin cytoskeleton, and extracellular matrix interactions (Figure S3B and Figure S4E). Collectively, these results highlight the importance of H2BK5Ac in regulating the active gene transcription program of TS cells, whereby loss of H2BK5Ac results in repression of genes critical to maintenance of the epithelial phenotype.

TS^{KI4} Cells and Claudin-Low Breast Cancer Share EMT Properties
Recent studies have shown that the CL subtype of triple-negative breast cancer exhibits both mesenchymal and stem-like properties (Prat et al., 2010). Compared to the four other breast tumor subtypes (i.e., luminal A, luminal B, HER2-enriched, and basal-like), CL tumors have the lowest expression of epithelial differentiation markers CD24, EpCAM, and KRT7/19 and the cell-adhesion proteins CLDN3/4/7 and CDH1, while exhibiting highest expression of the mesenchymal markers VIM, N-cadherin, SNAI2, and TWIST1 (Prat et al., 2010). Hierarchical clustering of 22 genes characteristic of EMT and stemness from gene expression data of TS^{KI4} cells and 52 breast cancer cells lines reported by Neve et al. (2006) revealed that TS^{KI4} cells clustered most closely with the CL breast cancer subtype (Figure 6A). Similar to the CL cell lines, TS^{KI4} cells exhibited an increase in the mesenchymal markers VIM, CDH2, SNAI2, and TWIST1 with loss of the epithelial differentiation and cell adhesion markers CD24, KRT7/8/19, and CLDN4 (Figure 6A). Next, we examined the intersection between genes with unique Entrez identifiers from gene array data of CL cell lines compared to gene array data of TS^{KI4} cells. The intersection between upregulated and downregulated genes in the CL cell lines compared to TS^{KI4} cells was determined to be significant with 62 upregulated (p value < 0.005) and 31 downregulated (p value < 0.01) overlapping genes (Figure 6B). This overlapping gene set was plotted on the basis of log$_2$ ratio values from TS^{KI4} cells to demonstrate gene expression changes of the intersecting TS^{KI4}/CL cell EMT gene signature (Figure 6C). Genes important for the induction of the mesenchymal phenotype—such as CDH2, DKK1, MET, PDGFRβ, SNAI2, TIMP2, THY1, TWIST1, and VIM—were significantly upregulated, while genes important for maintenance of the epithelial phenotype and cell adhesion—such as AIM1, BCAM, KRT7, KRT19, and RAB25—were repressed (Figure 6C). In addition to these known regulators of EMT, this significant genetic intersection between two distinct EMT models with stem cell characteristics highlights a gene set important for both EMT and stemness.

Epigenetic Repression of TS^{KI4}/CL EMT Genes by Reduction of H2BK5Ac
TS cell EMT models, TS^{KI4}, and TS^{Snail} demonstrated selective loss of histone H2A/H2BAc (Figure 4D). By H2BK5Ac ChIP-qRT-PCR, we examined the levels of H2BK5Ac on 32 downregulated genes that have overlapping gene expression profiles between CL SUM159 and TS^{KI4} cells and are known to
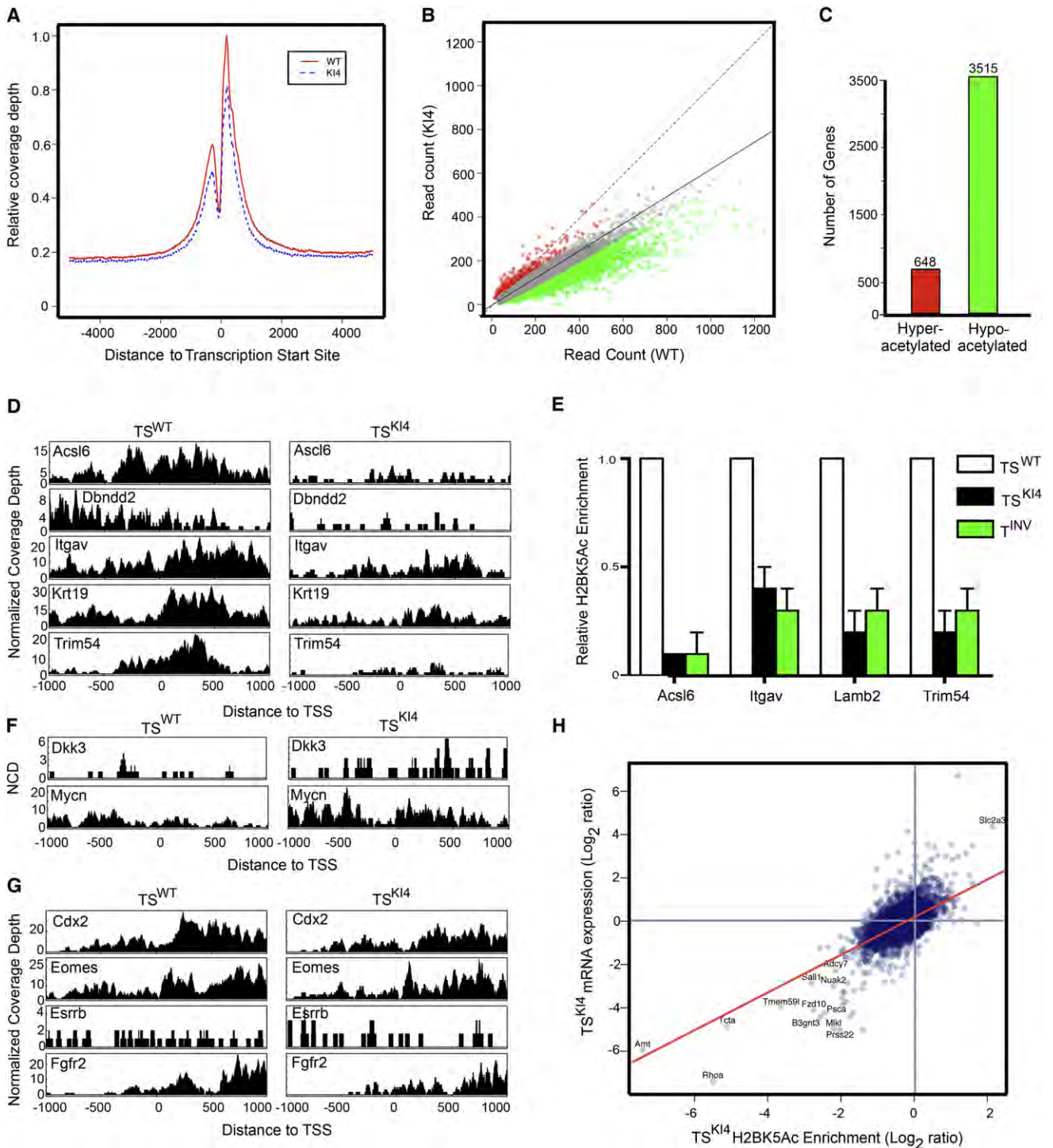
Figure 5. Reduction of H2BK5Ac on Select Promoters in TS^{KI4} Cells Contributes to Repression of the Epithelial Phenotype

(A) Peak H2BK5Ac density occurs within 1 kb of the TSS. Plot depicts the distribution of read tags around the TSS of mouse RefSeq genes. Solid red line represents the read tag distribution density of all genes in TS^{WT} cells, and dotted blue line represents TS^{KI4} cells. Data were pooled from two independent experiments sequenced in duplicate.

(B) Loss of H2BK5Ac occurs near the TSS of 3515 genes in TS^{KI4} cells. Scatter plot of RefSeq genes with read tag counts above 20 reads per 2 kb for genes identified from H2BK5Ac ChIP-seq of TS^{WT} (x axis) and TS^{KI4} (y axis) cells. Solid line represents the data normalization reference line for delineating genes with significant read count differences between TS^{WT} and TS^{KI4} cells. Significance is based upon Benjamini-Hochberg FDR adjusted p value $\leq$ 0.05. Green and red dots represent 3515 genes with a significant decrease and 648 genes with a significant increase in read tag density between TS^{WT} and TS^{KI4} cells, respectively. Gray dots represent all nonsignificantly changed genes. Dotted line is a 45° reference line.

have a significant loss of H2BK5Ac in TS[KI4] cells by ChIP-seq (Figure 6C and Table S3). Of the 32 genes tested by H2BK5Ac ChIP-qRT-PCR, 75% of these genes were validated to have a loss of H2BK5Ac and a coordinate loss of gene expression in TS[KI4] compared to TS[WT] cells (Figure 6D and Figures S5A–S5C). Furthermore, 81% of these genes had a similar loss of H2BK5Ac in TS[Snail] cells (Figure 6D and Figures S5B and S5C). Due to the significant genetic intersection between CL cell lines and the TS[KI4] EMT model, we determined the levels of H2BK5Ac on the promoters of the same 32 overlapping genes in the CL SUM159 cell line. Importantly, 80% of these genes had a loss of H2BK5Ac in SUM159 cells compared to human mammary epithelial cells (HMECs), as determined by ChIP-qRT-PCR (Figure 6E and Figures S5D and S5E). These results suggest that loss of H2BK5Ac represses genes with an important role in mainte- nance of the epithelial phenotype, thereby contributing to the progression of two distinct EMT programs.

The pathological significance of the TS[KI4]/CL association was further emphasized by comparing the gene expression profile of TS[KI4] cells to the five intrinsic molecular subtypes of breast tumors cataloged in the UNC337 data set (Prat et al., 2010). Tumors from the CL breast cancer subtype showed highest expression of the TS[KI4] gene expression signature compared to the basal-like, HER2-enriched, luminal A, and luminal B breast tumors (Figure 6F). Further analysis of the overlapping gene- expression profiles in CL human tumors and TS[KI4] cells demon- strated a highly significant intersection between the gene array profiles of TS[KI4] cells and CL human tumors (p value < 0.0001 for upregulated genes) (Figure 6G). Although the intersection between the downregulated genes from TS[KI4] cells and CL human tumors consists of only 13 genes, approximately 50% of these genes (AIM1, IRX5, KRT7, KRT19, RAB25, and SCYL3) were present in the intersecting TS[KI4]/CL EMT gene signature; these same genes also exhibited a coordinate loss of H2BK5Ac in TS[KI4] and CL cells (Figure 6D). These findings highlight the importance of H2BK5Ac on genes whose repression is important for EMT in both developmental stem cell and metastatic human tumor models of EMT with stem cell properties.

MAP3K4 Regulates CBP Acetylation of H2A and H2B

Previously, we showed the requirement of MAP3K4 kinase activity for neural tube, skeletal, and placental development (Abell et al., 2005, 2009). We systematically examined the MAP3K4 signaling network for genes whose targeted disruption resulted in phenotypes similar to those of KI4 mice (Table S5). Strikingly, the genes overlapping most closely with the develop- mental defects observed with loss of MAP3K4 kinase activity

were the histone acetyltransferase (HAT) CBP and its closely related family member p300. This phenotypic overlap suggested that the loss of H2A/H2BAc in TS[KI4] cells may be related to altered CBP and/or p300 HAT activity. Nuclear extracts isolated from TS[KI4] cells have significantly diminished HAT activity relative to TS[WT] cells (Figure 7A). Total CBP and p300 protein expression was unchanged in TS[KI4] cells (Figure S6A). MAP3K4-dependent JNK phosphorylation of CBP and p300 increased HAT activity, which was blocked by the JNK inhibitor SP600125 (Figure 7B and Figure S6B). TS[KI4] cells have a strongly diminished JNK activity (Abell et al., 2009), consistent with MAP3K4-dependent JNK activation regulating CBP/p300 HAT activity. Coexpression of MAP3K4 and JNK resulted in a 17.8- and 8.3-fold increase in the phosphorylation of CBP and p300, respectively (Figure 7C and Figure S6C). CBP/p300 phosphory- lation was JNK dependent, as p38 activation did not significantly alter phosphorylation of CBP or p300 (Figure 7C and Figure S6C). To determine if CBP or p300 regulate endogenous TS cell func- tions, we infected TS[WT] cells with shRNAs to either CBP or p300. We achieved greater than 85% knockdown of CBP or p300 with three to four individual shRNAs for each (Figures 7D and 7E and data not shown). Unlike control virus-infected cells (Figure 7F), loss of CBP resulted in a dramatic change in morphology with TS[shCBP] cells exhibiting a front-back end polarized morphology (Figures 7G and 7H). In contrast, cells with loss of p300 main- tained a normal epithelial morphology (data not shown). Compared to control virus-infected cells, stemness markers in TS[shCBP] cells were unchanged for Eomes and FGFR2 and decreased by 25% for Cdx2 and Esrrβ (Figure S6E). Further, expression of the mesenchymal marker vimentin was increased at both the level of message and protein in TS[shCBP] cells (Fig- ure S6F and data not shown). Most importantly, TS[shCBP] cells exhibited a 5- to 15-fold increase in invasiveness as compared to control virus-infected cells (Figure 7I). Changes in morphology and the expression of mesenchymal markers combined with increases in invasiveness suggest that loss of CBP in TS[WT] cells induces EMT. Examination of histone acetylation in TS[shCBP] cells revealed the selective and specific loss of H2A/H2BAc (Fig- ure 7J). In contrast, loss of p300 resulted in a reduction in H3 and H4 acetylation, but did not affect H2A/H2BAc (Figure 7K). These data strongly suggest that CBP is the primary HAT that regulates H2A/H2BAc in TS cells and that the loss of H2A/ H2BAc is sufficient to induce EMT in TS cells.

Genes downregulated in the TS[KI4]/CL EMT gene signature were similarly decreased in TS[shCBP] cells (Figure S6G). Because TS[shCBP] cells exhibit the selective loss of H2A/H2BAc acetylation similar to TS[KI4] and TS[Snail] cells, (Figure 4D and Figure 7J), we

(C) Bar graph summarizes all genes in (B) with significantly altered H2BK5Ac density in TS[KI4] cells. Data for (B) and (C) were pooled as described in (A).

(D) Reduced H2BK5Ac near the TSS of specific genes in TS[KI4] cells. Plots of H2BK5Ac density compare the normalized coverage depth (NCD) of read tags around the TSS for indicated genes with loss of H2BK5Ac (p values ≤ $1e^{-18}$) between TS[WT] and TS[KI4] cells. The x axis for each subplot is the distance to TSS, and the y axis is the NCD of read tags.

(E) Validation of reduced H2BK5Ac on specific genes in both TS[KI4] and T[INV] cells shown by ChIP qRT-PCR of TS[WT], TS[KI4], and T[INV] cells. Data show the mean ± range of two independent experiments performed in duplicate.

(F) Genes with increased H2BK5Ac near the TSS in TS[KI4] cells plotted as described in (D).

(G) Plots of H2BK5Ac density comparing the NCD for stem cell markers between TS[WT] and TS[KI4] cells.

(H) Changes in H2BK5Ac correlates with altered gene expression in TS[KI4] cells. Scatter plot of 6722 RefSeq genes with read tag counts above 50 reads per 1 kb for genes identified by H2BK5Ac ChIP-seq (x axis) and mRNA-seq (y axis) in TS[KI4] cells. Read tag counts were converted to $\log_2$ ratio values for comparison. Solid red line represents the linear regression line of the data with a Pearson correlation coefficient of 0.62 (p value < 10^{-16}). Labeled dots are genes with a 4-fold change in both mRNA abundance and H2BK5Ac enrichment.
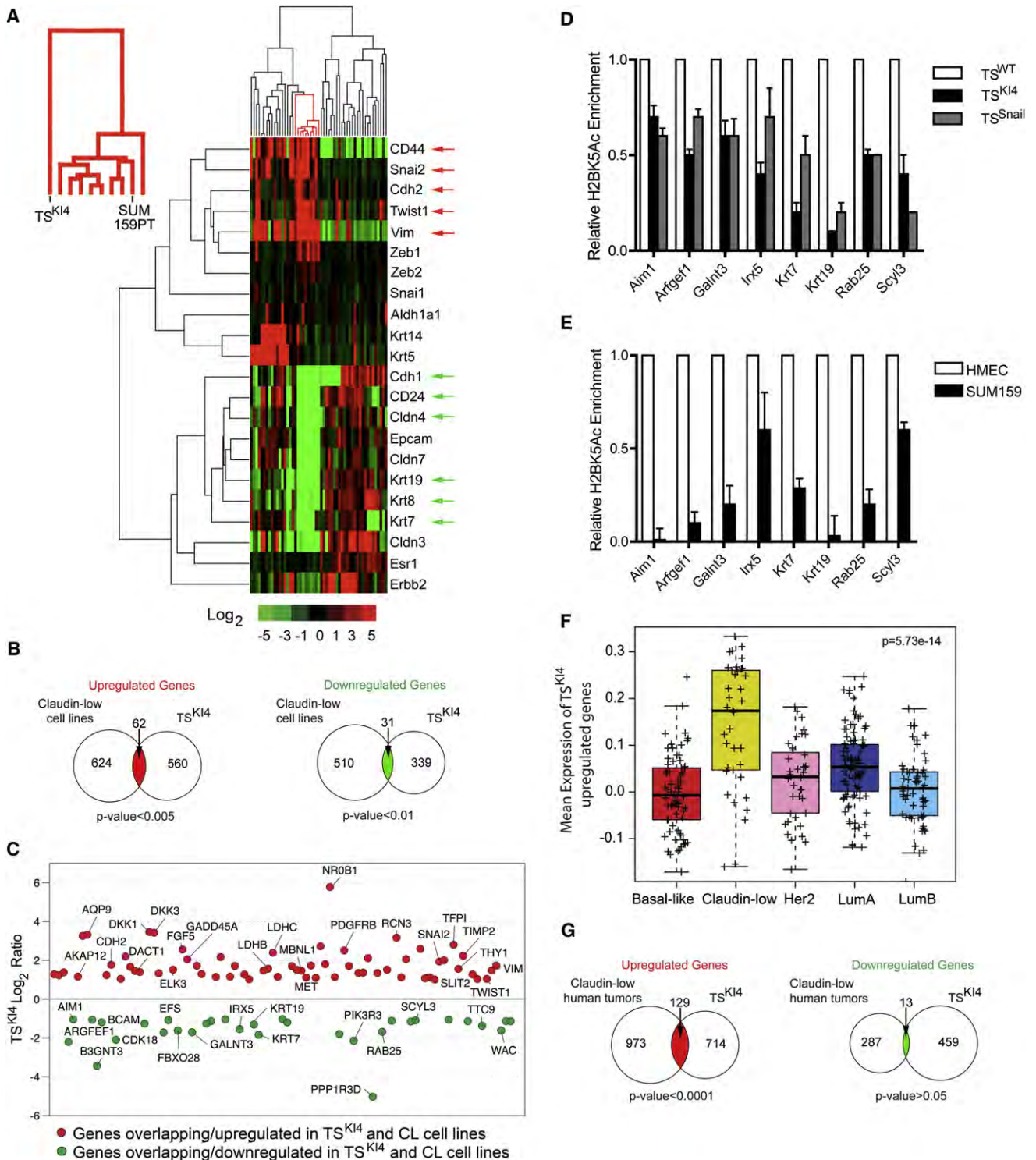
Figure 6. TS^KI4 Cells and Claudin-Low Breast Cancer with Properties of EMT and Stemness Show Loss of H2BK5Ac on Shared Genes

(A) TS^KI4 cells cluster with the CL subtype of breast cancer cells. Heat map compares expression of 22 breast cancer EMT genes in TS^KI4 cells and 52 breast cancer cell lines. TS^KI4 cell and CL breast cancer cluster is outlined in red. Red and green arrows indicate shared upregulated and downregulated genes respectively.

(B) Venn diagram depicts the intersection between genes elevated and downregulated in CL cell lines compared to TS^KI4 cells.

(C) Plot shows log$_2$ ratios (y axis) of TS^KI4 cells for intersecting genes depicted in (B).

(D) Reduced H2BK5Ac on specific genes in both TS^KI4 and TS^Snail cells from the intersecting downregulated genes in (C) measured by qRT-PCR of ChIP samples is shown.

used H2BK5Ac ChIP-qRT-PCR to measure H2BK5Ac on down-regulated genes from the intersecting TS[KI4]/CL gene profile (Figure S6G). Of these genes, 72% demonstrated a loss of H2BK5Ac in TS[shCBP] cells compared to control virus-infected cells (Figure S6H). These data show the coordinate loss of H2BK5Ac and gene expression in CL, TS[KI4], TS[Snail], and TS[shCBP] cells. Together, these findings show the importance of CBP-mediated H2BK5Ac in maintaining the epigenetic landscape important for the epithelial phenotype of TS cells.

DISCUSSION

We have shown that MAP3K4-dependent activation of JNK in response to FGF4 controls CBP activity for the maintenance of the TS cell epithelial phenotype. Loss of MAP3K4 kinase activity in TS[KI4] cells results in gain of EMT properties including reduced E-cadherin, and morphological changes characteristic of mesenchymal cells and increased invasiveness. TS[KI4] cells also retain stemness defined by self-renewal with the maintenance of multipotency. These properties of TS[KI4] cells show a functional separation of FGF4-dependent control of epithelial maintenance and stemness, with MAP3K4 signaling being critical for the epithelial phenotype.

TS[KI4] cells exhibit the selective loss of H2A/H2BAc, whereas histone H3 and H4 acetylation was largely unaffected. Loss of H2BK5Ac is restricted to a select set of genes in TS[KI4] cells whose expression is significantly reduced. Epithelial maintenance was also disrupted by CBP knockdown, causing the loss of H2A/H2BAc similar to that observed with TS[KI4] cells. Loss of CBP expression induced a phenotype similar to TS[KI4], including gain of invasiveness and EMT characteristics while maintaining stemness. Consistent with the novel role of CBP and H2BK5Ac in regulation of gene expression profiles important for the epithelial phenotype, H3K4me3 and H3K9me3 are unchanged in TS[KI4] cells. Additionally, H3K27me3 has been shown as unimportant in TS cell differentiation (Rugg-Gunn et al., 2010). Thus, histone acetylation by CBP is a primary mechanism for maintenance of the epithelial phenotype of TS cells, whereby loss of H2BK5Ac results in EMT. This finding is consistent with the role for CBP in maintaining hematopoietic stem cell self-renewal (Rebel et al., 2002). In addition to direct inhibition of CBP HAT activity, it is possible that a secondary mechanism of regulation exists to target loss of H2A/H2BAc to select gene promoters, whereby changes in CBP phosphorylation control interactions with transcriptional regulators of EMT (He et al., 2009).

Ectopic expression of Snail has been used to induce EMT in different cell types, and overexpression of Snail in HMECs induced a mesenchymal phenotype with expression of specific stem cell markers (Mani et al., 2008). This phenotype is reminiscent of TS[KI4] cells, which induce EMT while maintaining stemness. Stable expression of Snail in TS cells resulted in the selective loss of H2A/H2BAc and properties of EMT and stemness, similar to TS[KI4] and TS[shCBP] cells. ChIP-qRT-PCR studies showed loss of H2BK5Ac on an overlapping set of genes for TS[KI4], TS[shCBP], and TS[Snail] cells, defining each as a unique model system for the epigenetic control of EMT in a self-renewing primary cell.

In contrast to TS[KI4], TS[shCBP], and TS[Snail] cells, T[INV] cells have completed EMT, having fully lost their epithelial morphology, as evidenced by the increase in invasiveness and gain in the mesenchymal morphology associated with filamentous actin and increased expression of the mesenchymal marker fibronectin. T[INV] cells do not self-renew and have lost acetylation of all four core histones. Since T[INV] cells have completed EMT, T[INV] gene expression profiles probably lack the EMT initiators, instead showing the expression of EMT executors (Thiery et al., 2009). Compared to T[INV] cells, TS[KI4], TS[shCBP], and TS[Snail] cells are in an intermediate state of EMT, where they are not fully mesenchymal, but exhibit properties of both EMT and stemness. TS[KI4] cells are uniquely trapped in this intermediate EMT state prior to complete acquisition of the mesenchymal phenotype, which can still be induced by the removal of FGF4.

TS cell EMT shares many key properties with neural crest and cancer cell EMTs including loss of E-cadherin, gain of front-to-back polarity, and increased invasiveness (Yang and Weinberg, 2008). However, there are differences in marker expression among these different EMT models, indicative of cell type and stage-specific EMT. For example, mesenchymal markers such as vimentin and N-cadherin are differentially expressed in these different EMT models, with N-cadherin repression being required for neural crest EMT (Yang and Weinberg, 2008). Lamb2 is increased in hepatocyte EMT, but reduced in neural crest, CL, T[INV], TS[KI4], and TS[Snail] EMTs. Fibronectin is elevated in breast and gastric cancers and in T[INV] cells, but reduced in TS[KI4] and TS[Snail] cells. The critical property for each EMT model is increased invasiveness (Kalluri and Weinberg, 2009).

Finally, TS[KI4] and CL human breast cancer cells share properties of stemness and EMT with a common gene expression profile also found in patient CL tumors. Intersecting genes with loss of expression had a correlative loss of H2BK5Ac in both TS[KI4] and CL cells. Some of these genes have defined roles in maintenance of the epithelial phenotype such as Aim1, Rab25, and Galnt3 (Maupin et al., 2010; Ray et al., 1997), but most of the shared genes in the TS[KI4]/CL intersecting list have not been characterized for their role in epithelial maintenance or EMT and should be analyzed in different EMT models. Discovery of how H2A/H2BAc controls maintenance of the epithelial TS cell phenotype provides unique insight into how signaling networks controlling tissue stem cell EMT can be used to define previously unrecognized genes contributing to cancer cell EMT. This discovery may lead to defining novel gene targets or

(E) Reduced H2BK5Ac on specific genes in CL breast cancer lines compared to normal HMEC breast cells as measured by ChIP-qRT-PCR. (D and E) Data are the mean ± range of two independent experiments performed in duplicate.
(F) CL human tumors show the highest expression of TS[KI4] genes among breast cancer subtypes. Mean expression of TS[KI4] cell upregulated genes across the subtypes of breast cancer in the UNC337 data set. p value was calculated by comparing gene expression means across all subtypes using an ANOVA test. Each (+) represents a distinct tumor sample within the data set.
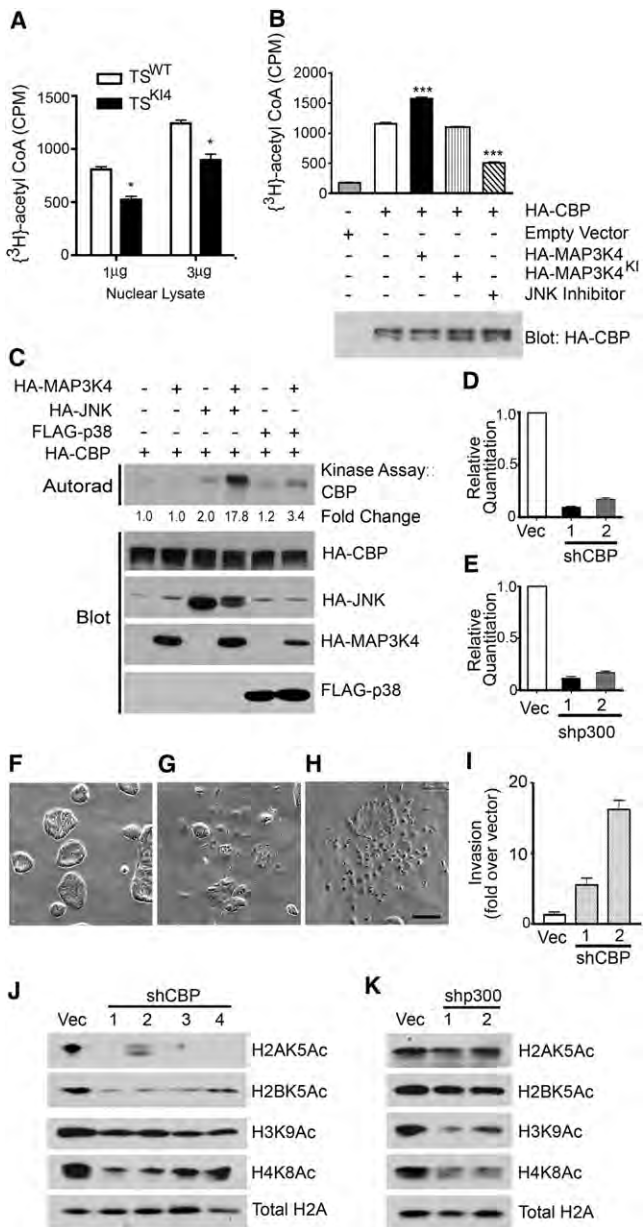(G) Venn diagram of intersecting genes elevated and downregulated in CL human tumors and TS[KI4] cells.

combinations of targets whose inhibition can be used to selectively inhibit TICs.

EXPERIMENTAL PROCEDURES

Cell Lines, Culture Conditions, and Transfections

TS^{WT} and TS^{KI4} cells of normal karyotype were isolated from heterozygote crosses of mice with a targeted mutation of MAP3K4 (K1361R) as previously described (Abell et al., 2009). TS cells were cultured without feeders in 30% TS media (RPMI 1640, 20% fetal bovine serum, 1% penicillin and streptomycin, 1% L-glutamine, 1% sodium pyruvate, and 100 μM β-mercaptoethanol) and 70% MEF-conditioned TS cell media, supplemented with FGF4 (37.5 ng/ml) and Heparin (1 mg/ml). For differentiation, TS cells were cultured in TS media only. Invasion assays, isolation of T^{INV} cells, HEK293 cell culture, transfection, and plasmids are specified in Supplemental Experimental Procedures.

Western Blotting of Whole-Cell, Nuclear, and Histone Lysates

Whole-cell and nuclear lysates were isolated as previously described (Abell et al., 2009). For histone lysates, cells were lysed on ice in buffer containing PBS, 1% Triton-X, and 1 mM PMSF. Pellets were spun at 2000 rpm for 10 min at 4°C and extracted overnight in 0.2 N HCl with shaking at 4°C. Western blots were performed with the antibodies specified in Supplemental Experimental Procedures.

In Vitro Histone Acetyltransferase, Immunoprecipitation, and Kinase Assays

HAT assays and kinase assays were performed as described in Supplemental Experimental Procedures.

Chromatin Immunoprecipitation Coupled to High Throughput Sequencing

Cells were fixed for 10 min in 1% formaldehyde, sonicated (VCX130 Ultrasonicator), and immunoprecipitated with 5 μg anti-H2BK5Ac and Protein A dynabeads (Invitrogen) (Wang et al., 2008). Crosslinking was reversed by overnight incubation at 65°C. DNA was purified with the MinElute PCR purification kit (QIAGEN). Library preparation for Illumina ChIP-seq was performed according to manufacturer's instructions (Illumina). Illumina Solexa GA II was used to produce ~36 bp sequence reads, which were mapped to the mouse genome using Mapping and Alignment with Quality (MAQ) software in conjunction with EpiCenter for comparative analysis as described in Supplemental Experimental Procedures. PCR conditions and primers used for ChIP-seq validation are described in Supplemental Experimental Procedures.

Real-Time Quantitative RT-PCR, Agilent Gene Expression Arrays, Comparative Expression, and GO Pathway Analysis

Total RNA was isolated using RNeasy Plus minikit (QIAGEN). cDNA was synthesized from 3 μg RNA using High-Capacity reverse transcription kit (Applied Biosystems). Applied Biosystems 7500 RT-PCR system with invitoried TaqMan probes was used to quantify gene-expression levels normalized to β-actin expression. Agilent Gene Expression Arrays, Comparative

Figure 7. CBP Expression is Required for MAP3K4-Dependent Regulation of the Epithelial Phenotype in TS Cells

(A) HAT activity is significantly decreased in TS^{KI4} cells. Activity of 1 or 3 μg of nuclear lysate isolated from TS^{WT} or TS^{KI4} cells is measured. Significance of change in HAT activity was evaluated by an unpaired Student's t test, *p value < 0.05.

(B) MAP3K4/JNK increases HAT activity of CBP measured as incorporation of [^{3}H]-acetyl-CoA in counts per minute (CPM) in 293 cells coexpressing CBP with the constitutively active kinase domain of MAP3K4 or kinase-inactive (KI). Significance of change in HAT activity was evaluated by an unpaired Student's t test. ***p value < 0.001; *p value < 0.05. Data represent the mean ± SEM of three independent experiments performed in triplicate.

(C) MAP3K4 and JNK promote phosphorylation of CBP as measured by kinase assay. γ-^{32}P-labeled ATP proteins were visualized by autoradiography and quantified by phosphorimaging. Data are representative of two independent experiments.

(D and E) qRT-PCR shows reduced expression of CBP and p300 in TS^{WT} cells infected with unique shRNAs for CBP (D) or p300 (E) compared to control

virus-infected cells (Vec). Data represent the mean ± range of two independent experiments performed in triplicate.

(F–H) shRNA knockdown of CBP results in loss of the epithelial phenotype. Phase microscopy shows morphology of control virus-infected cells (F) compared to mesenchymal morphology of cells expressing CBP shRNAs (G and H). Black bar represents 100 μm.

(I) Increased invasiveness of shCBP expressing cells compared to control virus-infected cells. Data shown represent the mean ± range of two independent experiments performed in triplicate.

(J and K) Selective loss of H2A/H2BAc in CBP knockdown cells. Western blotting of lysates from TS^{WT} cells infected with control virus, four independent CBP shRNAs (J) or two independent p300 shRNAs is shown. Results are representative of two independent experiments.

Expression, and GO Pathway Analysis were performed as described in Supplemental Experimental Procedures.

Immunofluorescence

Immunostaining was performed as described in Supplemental Experimental Procedures.

ACCESSION NUMBERS

The accession number for the microarray data is GSE27883.

SUPPLEMENTAL INFORMATION

Supplemental Information includes six figures, five tables, and Supplemental Experimental Procedures and can be found with this article online at doi:10.1016/j.stem.2011.03.008.

REFERENCES

Abell, A.N., Rivera-Perez, J.A., Cuevas, B.D., Uhlik, M.T., Sather, S., Johnson, N.L., Minton, S.K., Lauder, J.M., Winter-Vann, A.M., Nakamura, K., et al. (2005). Ablation of MEKK4 kinase activity causes neurulation and skeletal patterning defects in the mouse embryo. Mol. Cell. Biol. 25, 8948–8959.

Abell, A.N., Granger, D.A., Johnson, N.L., Vincent-Jordan, N., Dibble, C.F., and Johnson, G.L. (2009). Trophoblast Stem Cell Maintenance by Fibroblast Growth Factor 4 Requires MEKK4 Activation of Jun N-Terminal Kinase. Mol. Cell. Biol. 29, 2748–2761.

Cano, A., Pérez-Moreno, M.A., Rodrigo, I., Locascio, A., Blanco, M.J., del Barrio, M.G., Portillo, F., and Nieto, M.A. (2000). The transcription factor snail controls epithelial-mesenchymal transitions by repressing E-cadherin expression. Nat. Cell Biol. 2, 76–83.

He, S., Nakada, D., and Morrison, S.J. (2009). Mechanisms of stem cell self-renewal. Annu. Rev. Cell Dev. Biol. 25, 377–406.

Kalluri, R., and Weinberg, R.A. (2009). The basics of epithelial-mesenchymal transition. J. Clin. Invest. 119, 1420–1428.

Lim, E., Vaillant, F., Wu, D., Forrest, N.C., Pal, B., Hart, A.H., Asselin-Labat, M.-L., Gyorki, D.E., Ward, T., Partanen, A., et al. (2009). Aberrant luminal progenitors as the candidate target population for basal tumor development in BRCA1 mutation carriers. Nature Medicine 15, 907–913.

Mani, S.A., Guo, W., Liao, M.-J., Eaton, E.N., Ayyanan, A., Zhou, A.Y., Brooks, M., Reinhard, F., Zhang, C.C., Shipitsin, M., et al. (2008). The epithelial-mesenchymal transition generates cells with properties of stem cells. Cell 133, 704–715.

Maupin, K.A., Sinha, A., Eugster, E., Miller, J., Ross, J., Paulino, V., Keshamouni, V.G., Tran, N., Berens, M., Webb, C., and Haab, B.B. (2010). Glycogene Expression Alterations Associated with Pancreatic Cancer Epithelial-Mesenchymal Transition in Complementary Model Systems. PLoS ONE 5, e13002.

Neve, R.M., Chin, K., Fridlyand, J., Yeh, J., Baehner, F.L., Fevr, T., Clark, L., Bayani, N., Coppe, J.-P., Tong, F., et al. (2006). A collection of breast cancer cell lines for the study of functionally distinct cancer subtypes. Cancer Cell 10, 515–527.

Niwa, H., Toyooka, Y., Shimosato, D., Strumpf, D., Takahashi, K., Yagi, R., and Rossant, J. (2005). Interaction between Oct3/4 and Cdx2 determines trophectoderm differentiation. Cell 123, 917–929.

Norwitz, E.R., Schust, D.J., and Fisher, S.J. (2001). Implantation and the survival of early pregnancy. N. Engl. J. Med. 345, 1400–1408.

Prat, A., Parker, J.S., Karginova, O., Fan, C., Livasy, C., Herschkowitz, J.I., He, X., and Perou, C.M. (2010). Phenotypic and molecular characterization of the claudin-low intrinsic subtype of breast cancer. Breast Cancer Res. 12, R68.

Ray, M.E., Wistow, G., Su, Y.A., Meltzer, P.S., and Trent, J.M. (1997). AIM1, a novel non-lens member of the betagamma-crystallin superfamily, is associated with the control of tumorigenicity in human malignant melanoma. Proc. Natl. Acad. Sci. USA 94, 3229–3234.

Rebel, V.I., Kung, A.L., Tanner, E.A., Yang, H., Bronson, R.T., and Livingston, D.M. (2002). Distinct roles for CREB-binding protein and p300 in hematopoietic stem cell self-renewal. Proc. Natl. Acad. Sci. USA 99, 14789–14794.

Rugg-Gunn, P.J., Cox, B.J., Ralston, A., and Rossant, J. (2010). Distinct histone modifications in stem cell lines and tissue lineages from the early mouse embryo. Proc. Natl. Acad. Sci. USA 107, 10783–10790.

Tanaka, S., Kunath, T., Hadjantonakis, A., Nagy, A., and Rossant, J. (1998). Promotion of Trophoblast Stem Cell Proliferation by FGF4. Science 282, 2072–2075.

Thiery, J.P., Acloque, H., Huang, R.Y.J., and Nieto, M.A. (2009). Epithelial-mesenchymal transitions in development and disease. Cell 139, 871–890.

Wang, Z., Zang, C., Rosenfeld, J.A., Schones, D.E., Barski, A., Cuddapah, S., Cui, K., Roh, T.-Y., Peng, W., Zhang, M.Q., and Zhao, K. (2008). Combinatorial patterns of histone acetylations and methylations in the human genome. Nat. Genet. 40, 897–903.

Yang, J., and Weinberg, R.A. (2008). Epithelial-mesenchymal transition: at the crossroads of development and tumor metastasis. Dev. Cell 14, 818–829.

of the gene-expression changes in the patient-derived iPSCs, including reducing expression of the schizophrenia risk gene *TCF4* to normal levels. Again, the availability of living neurons permitted these examinations. The ability to differentiate iPSCs into diverse cell types, including oligodendrocytes, which have previously been implicated in schizophrenia (Takahashi et al., 2011), will permit a broad look at cellular alterations that take place in psychiatric and neurological diseases. We can now look forward to a much better understanding of the relationship between genetic risk factors, gene-expression changes, and neuronal and glial function in schizophrenia, as well as opportunities to perform high-throughput screening of compound libraries in patient-derived neuronal and glial cells as a step toward relevant drug discovery.

While this effort from Brennand et al. (2011) is just a beginning, the now widespread availability of fibroblasts (and other cells) from patients with schizophrenia and other complex disorders will undoubtedly lead to very large-scale studies using assays such as those employed by Brennand et al. (2011). The authors suggest that with the examination of an increasing number of patient-derived lines, the list of consistently affected genes will be diminished. In our opinion, the addition of future studies will likely lead to subgrouping of iPSCs, based on the patterns of pathways that are impacted in each case. In disorders such as schizophrenia with high heritability, determining the relationship between the genetic variations present in the iPSCs that cluster to each of these subgroups will then permit the prospective assignment of individual patients to a given subgroup, based solely on results of DNA sampling. The opportunity to identify interventions that are most effective in specific subgroups represents the ultimate promise of individualized medicine in complex disease.

REFERENCES

Brennand, K.J., Simone, A., Jou, J., Gelboin-Burkhart, C., Tran, N., Sangar, S., Li, Y., Mu, Y., Chen, G., Yu, D., et al. (2011). Nature. 10.1038/nature09915.

Dean, B., Boer, S., Gibbons, A., Money, T., and Scarr, E. (2009). Curr. Opin. Psychiatry *22*, 154–160.

Deep-Soboslay, A., Benes, F.M., Haroutunian, V., Ellis, J.K., Kleinman, J.E., and Hyde, T.M. (2011). Biol. Psychiatry *69*, 104–112.

Insel, T.R. (2010). Nature *468*, 187–193.

Koenen, K.C., Moffitt, T.E., Roberts, A.L., Martin, L.T., Kubzansky, L., Harrington, H., Poulton, R., and Caspi, A. (2009). Am. J. Psychiatry *166*, 50–57.

Owen, M.J., Craddock, N., and O'Donovan, M.C. (2010). Arch. Gen. Psychiatry *67*, 667–673.

Purcell, S.M., Wray, N.R., Stone, J.L., Visscher, P.M., O'Donovan, M.C., Sullivan, P.F., and Sklar, P. (2009). Nature *460*, 748–752.

Sebat, J., Levy, D.L., and McCarthy, S.E. (2009). Trends Genet. *25*, 528–535.

Takahashi, N., Sakurai, T., Davis, K.L., and Buxbaum, J.D. (2011). Prog. Neurobiol. *93*, 13–24.

An Epigenetic Mark that Protects the Epithelial Phenotype in Health and Disease

Fabiana Heredia[1] and M. Angela Nieto[1,*]
[1]Instituto de Neurociencias CSIC-UMH, Avda. Ramón y Cajal s/n, 03550 San Juan de Alicante, Spain
*Correspondence: anieto@umh.es
DOI 10.1016/j.stem.2011.04.011

Epithelial plasticity is crucial during embryonic development and progression of carcinomas. In this issue, Abell et al. (2011) show that acetylation on histones H2A/H2B prevents epithelial cells from undergoing epithelial-to-mesenchymal transition (EMT). Their findings also suggest that under conditions where EMT and stemness coexist, they can be independently regulated.

Epithelial plasticity is the biological mechanism underlying organ formation. During embryonic development, many tissues and organs originate after one or several rounds of EMT and the reverse process, mesenchymal-to-epithelial transition, or MET. In adulthood, epithelial homeostasis is instead important to maintain tissue architecture, and reactivation of the EMT program is associated with progression of carcinomas and organ fibrosis (Thiery et al., 2009). Recent work suggests that cancer progression and reactivation of developmental programs such as EMT are both associated with acquisition of stem cell properties. Indeed, poorly differentiated and invasive human tumors in addition to expressing EMT markers also show an embryonic stem cell (ESC) signature (Ben-Porath et al., 2008). Furthermore, inducing EMT in mammary epithelial cells by overexpressing transcription factors Snail or Twist has been shown to confer stem cell properties (Mani et al., 2008). However, the reverse process, MET, has also been reported to be an important component, driving reprogramming of fibroblasts to induced pluripotent stem cells (iPSCs) (Li et al., 2010; Samavarchi-Tehrani et al., 2010), findings which suggest that the interrelationship between stem cell properties and EMT or MET is complex. In this issue of *Cell Stem Cell*, Abell et al. (2011) use trophoblast stem (TS) cells as a model system to confirm that stem cell properties and EMT signatures coexist in a developmental context as well as in cancer cells. They also report that histone 2A/2B acetylation represents

a specific epigenetic mark that is lost during EMT without affecting stem cell properties, suggesting that EMT and stemness can be independently regulated.

As TS cells differentiate and lose their stem cell properties, they undergo EMT and acquire invasive properties to enable embryo implantation. In vitro, they can be maintained indefinitely as self-renewing epithelial colonies in the presence of FGF4, and removing FGF4 will induce their differentiation toward placental subtypes. In previous work, Abell and colleagues showed that mice with an inactivating mutation in MAP3K kinase (KI4$^{-/-}$ mice) had abnormal placental development characterized by increased trophoblast invasion (Abell et al., 2009). Trophoblast stem cells derived from the KI4$^{-/-}$ mice, TSKI4 cells, are multipotent and not only self-renew in the presence of FGF4, but also exhibit EMT characteristics, suggesting that they represent stem cells that have lost the epithelial state.

Making use of an invasion assay, Abell et al. (2011) separated TS cells that had undergone EMT and compared their expression profile to that of TSKI4 and noninvasive TS cells. After clustering of the results and the generation of Venn diagrams, the authors found numerous shared genes, some of them already known to participate in regulation of the epithelial phenotype, and others not yet related to EMT and invasion, which might be important to analyze during cancer progression. The authors next looked at acetylation of histones and found that although FGF4 withdrawal induced loss of acetylation on all core histones in wildtype TS cells, a selective loss of acetylation on histones H2A and H2B was observed in the TSKI4 cells. In an analogous experiment, Abell et al. (2011) found that TS cells overexpressing Snail, which also have properties of stemness combined with EMT, also lose this epigenetic mark. Combining chromatin immunoprecipitation (ChIP)-seq with mRNA-seq analysis revealed that loss of H2B acetylation was associated with repression of genes required to maintain the epithelial phenotype. The authors next identified the histone acetyl transferase CBP as a candidate regulator in this context, based on the phenotypic similarity between MAP3K4 (KI4) and

CBP/p300$^{-/-}$ mice. Indeed, CBP knockdown in TS cells induced a selective and specific loss of the H2A/H2B mark and an expression profile correlating with the TSKI4 cells. Taken together, these findings suggest that the regulation of H2B/2A acetylation specifically affects epithelial plasticity and that the MAP3K4/CBP axis controls the active chromatin states of the promoters of "epithelial" genes, maintaining cells in an epithelial state protected from undergoing EMT.

An interesting aspect of this work is that a similar EMT signature and the absence of the H2BK5Ac epigenetic mark is also present in a type of breast cancer, the claudin-low type (CL), recently shown to exhibit both EMT and stem-like properties (Prat et al., 2010). In relation to this, it is interesting to note that even though breast carcinomas of the aggressive basal-type undergo EMT (Sarrió et al., 2008), they do not seem to share the gene signature found both in the claudin-type and the TS-EMT models presented in this work, posing the question as to whether different carcinoma types can progress toward the EMT following different programs.

With respect to the intersection between EMT and stemness, the findings of the present work suggest that specific mechanisms operate to control EMT in TS cells without affecting stem cell properties. However, a more detailed understanding of the mechanistic relationship between EMT and stemness is a topic for future investigation, as even the operational definition of stem cell properties varies in different biological contexts. While embryonic stem cells (ESCs) are defined by their ability to contribute to all embryonic lineages, TS cells are multipotent in the sense that they are restricted to give rise to different extraembryonic tissues. Cancer stem cells (CSCs), on the other hand, have characteristics associated with normal stem cells, but are defined by their ability to give rise to all cell types found in a particular cancer sample in serial transplants. It is obvious that these three criteria are not identical and that the degree of pluripotency varies depending on the system. Pluripotency in itself does not seem to be crucial for cancer progression, as cancer cells during metastasis formation only revert

to the phenotypes of the primary carcinoma. Therefore, as pluripotency and stemness are not interchangeable, the dynamics of epithelial plasticity and EMT during either reprogramming to iPSCs or normal TS differentiation and during cancer progression may be different (Ocaña and Nieto, 2010). Last, but not least, it is important to keep in mind that the process of EMT during both embryonic development and cancer progression is usually a transient state not associated with a particular cell fate, as MET is necessary for both the formation of many organs and distant metastasis. In contrast, cell differentiation in terms of the acquisition of a particular fate concomitant with the loss of pluripotency is a process that may occur simultaneously with EMT, but not necessarily linked to it. We will surely hear much more about these crucial issues in the next few years.

REFERENCES

Abell, A.N., Granger, D.A., Johnson, N.L., Vincent-Jordan, N., Dibble, C.F., and Johnson, G.L. (2009). Mol. Cell. Biol. 29, 2748–2761.

Abell, A., Jordan, N.V., Huang, W., Prat, A., Midland, A.A., Johnson, N.L., Granger, D.A., Mieczkowski, P.A., Perou, C.M., Gomez, S.M., et al. (2011). Cell Stem Cell 8, this issue, 525–537.

Ben-Porath, I., Thomson, M.W., Carey, V.J., Ge, R., Bell, G.W., Regev, A., and Weinberg, R.A. (2008). Nat. Genet. 40, 499–507.

Li, R., Liang, J., Ni, S., Zhou, T., Qing, X., Zhou, A.Y., Brooks, M., Reinhard, F., Zhang, C.C., Li, R., et al. (2010). Cell Stem Cell 7, 51–63.

Mani, S.A., Guo, W., Liao, M.J., Eaton, E.N., Ayyanan, A., Zhou, A.Y., Brooks, M., Reinhard, F., Zhang, C.C., Shipitsin, M., et al. (2008). Cell 133, 704–715.

Ocaña, O.H., and Nieto, M.A. (2010). Cell Res. 20, 1086–1088.

Prat, A., Parker, J.S., Karginova, O., Fan, C., Livasy, C., Herschkowitz, J.I., He, X., and Perou, C.M. (2010). Breast Cancer Res. 12, R68. 10.1186/bcr2635.

Samavarchi-Tehrani, P., Golipour, A., David, L., Sung, H.K., Beyer, T.A., Datti, A., Woltjen, K., Nagy, A., and Wrana, J.L. (2010). Cell Stem Cell 7, 64–77.

Sarrió, D., Rodriguez-Pinilla, S.M., Hardisson, D., Cano, A., Moreno-Bueno, G., and Palacios, J. (2008). Cancer Res. 68, 989–997.

Thiery, J.P., Acloque, H., Huang, R.Y., and Nieto, M.A. (2009). Cell 139, 871–890.